RSC Advances

PAPER

View Article Online
View Journal | View Issue

Cite this: *RSC Adv.*, 2017, **7**, 13272

Micrometre-length continuous single-crystalline nm-thin Fe_3C-nanowires with unusual 010 preferred orientation inside radial few-wall carbon nanotube structures: the key role of sulfur in viscous boundary layer CVS of ferrocene†

Filippo S. Boi,*[a] Jiayu Wang,[a] Sameera Ivaturi,[a] Xi Zhang,[a] Shanling Wang,[b] Jiqiu Wen,[b] Yi He[b] and Gang Xiang*[a]

Received 7th January 2017
Accepted 15th February 2017

DOI: 10.1039/c7ra00240h

rsc.li/rsc-advances

A key challenge in the fabrication of carbon nanotubes filled with ferromagnetic nanowires is the control of the number of nanotube-walls together with the nanowire continuity, composition and crystallinity. We report the serendipitous observation of novel radial carbon nanotube structures with few walls (2–5 walls) filled with nm-thin and many-micrometres long continuous single-crystalline Fe_3C nanowires. These are the dominant reaction products in chemical vapour synthesis experiments involving the pyrolysis of ferrocene/sulfur mixtures in the viscous boundary layer between a rough surface and a laminar Ar flow. These nanowires are found with an unusual preferred 010 orientation along the nanotube capillary. The properties of these structures are investigated through the use of multiple techniques: SEM, TEM, HRTEM, EDX, STEM, XRD, Raman spectroscopy, FT-IR spectroscopy and VSM.

Introduction

For more than a decade, carbon nanotubes (CNTs) have attracted a great deal of attention thanks to their exceptional physical, mechanical and chemical properties.[1–3] These nanostructures have been considered ideal for numerous applications such as black body absorbers,[4] electrodes,[5,6] aerogels,[5,6] buckypaper membranes,[7,8] capacitors[5–8] and many others. In this context, thanks to their great chemical stability, CNTs have also been considered ideal candidates for the encapsulation of ferromagnetic materials to protect them from oxidation. CNTs partially filled with ferromagnetic nanowires like α-Fe or Fe_3C have been reported in numerous studies as products of the chemical vapour deposition (CVD) of ferrocene.[9] However one of the major challenges in the growth of these types of structures is the control of the nanowire length, continuity and composition together with the control of the number of CNT walls. Recent studies have shown that the control of the nanowire continuity can be achieved through different strategies. Three main approaches have been proposed: (1) a perturbed low flow-rate chemical vapour synthesis (CVS)-type approach,[10,11] (2) a T-gradient driven low flow-rate approach involving the encapsulation of continuous α-Fe-nanowires inside vertically aligned multiwall CNT (MWCNT) films;[12] and (3) a Cl-assisted laminar CVD approach.[13–20] In the first approach, developed in 2013 by Boi *et al.*, it has been shown that the presence of local perturbations in a pyrolysed ferrocene vapour with high concentration of Fe and C species (in conditions of low vapour flow-rates) can allow the fabrication of radial-MWCNT structures and flower-like CNT structures characterized by continuous Fe-filling rates in the order of many micrometres.[10,11]

Specifically, in the radial structure case,[10] it was shown that the formation of a viscous boundary layer between a rough surface and a pyrolysed ferrocene vapour can allow the spontaneous homogeneous nucleation of Fe-particles in the vapour, and the subsequent formation of CNTs and encapsulation of Fe driven by a temperature gradient formed at the open CNTs-tip.[10] Similarly, a homogeneous nucleation mechanism was also observed in the case of the flower-like CNT structures for different types of substrate roughness (k-type like roughness).[11] A T-gradient driven growth mechanism (driven by a temperature gradient at the open CNT tip) was also reported by Peci *et al.*[12] in the case of the second approach. Despite the very high ferromagnetic filling rates achievable with these types of methods, the presence of a large quantity of CNT walls around the nanowires has limited the development of these types of materials for possible applications in thermoelectric systems, where the number of CNT-walls and CNT-chirality has been reported to play a crucial role.[21–30] Indeed high Seebeck coefficients have been reported in the case of composites fabricated

[a]College of Physical Science and Technology, Sichuan University, Chengdu, China. E-mail: f.boi@scu.edu.cn; gxiang@scu.edu.cn

[b]Analytical and Testing Center, Sichuan University, Chengdu, China

† Electronic supplementary information (ESI) available. See DOI: 10.1039/c7ra00240h

with semiconducting single wall CNTs (SWCNTs).[31] Differently from the first and second approaches, in the third approach the use of Cl radicals has been proven to have a key role in promoting the ferromagnet-encapsulation process by slowing-down the CNT growth mechanism through the removal of carbon feedstock and formation of CCl_4 species.[13–20] The use of Cl radicals has attracted a great deal of attention for the fabrication of randomly oriented or horizontally aligned films of thin walled CNTs characterized by high ferromagnetic filling rates and excellent magnetic properties. In these methods the Cl concentration has also been reported to play a key role in the control of the number of CNT-walls, allowing the synthesis of buckypapers composed of highly filled CNTs with approximately 9–10 walls.[18] Interestingly, recent studies have also shown that sulfur can be considered a useful growth-promoter for the fabrication of empty carbon nanostructures with different types of morphologies: Y-junctions, urchin-like structures, single wall CNT (SWCNT) strands, double-walled CNT films, amorphous CNTs, and other types of CNT morphologies with variable number of diameters, lengths and walls.[21–28] In addition, recent reports have also shown that sulfur can be used for the fabrication of large scale SWCNT films and composites.[29–31] In these experiments the dependence of the CNT diameter on the sulfur concentration has been proposed. It has been shown that for CNTs grown from heterogeneously nucleated particles, the local Fe–S–Fe eutectic active areas with diameters much smaller than that of the catalyst particles can allow for the control of CNT-diameters. Note that only very low quantities of sulfur have been reported to be involved in the CNT-fabrication process.[32] Given the role of sulfur as the selective growth-promoter for thin walled CNT fabrication, the use of these species was considered for experiments performed in the viscous boundary layers. The use of Cl species was not chosen since it would slow-down the CNT-growth and lead to the disappearance of the open-tip temperature-gradient driven mechanism which is characteristic of the radial structure growth as mentioned in approach 1.[10]

In this work we report the serendipitous observation of radial few wall (2–5 walls) carbon nanotube structures continuously filled with nm-thin Fe_3C nanowires as the dominant reaction product in the CVS experiments involving the pyrolysis of ferrocene/sulfur mixtures in the viscous boundary layer between a rough surface and a laminar Ar flow. We find that the presence of small quantities of sulfur in the viscous boundary layer has a dramatic effect on the growth mechanism of the radial structures and leads to a considerable decrease of the nucleated CNT-diameter. We demonstrate the continuity of the Fe_3C nanowires and single crystalline arrangement with the use of transmission electron microscopy (TEM), high resolution TEM (HRTEM), electron diffraction (ED) and scanning TEM (STEM). These nanowires are found with an unusual 010 preferred orientation. The structural arrangement of the radial structures is then also investigated through X-ray diffraction (XRD), Raman Spectroscopy (RS) and Fourier-transform infrared spectroscopy (FT-IR). The magnetic properties of the as-grown structures are investigated through vibrating sample magnetometry (VSM).

Experimental

The samples were synthesised as follows: 80–180 mg of ferrocene and 4 mg of sulfur were sublimated and pyrolysed in a CVD reactor consisting of a quartz tube of 1.5 m length, 2.5 mm thickness and a one-zone electrical furnace set at the temperature of 990 °C. The precursors were sublimated at the temperature of 350 °C. The rough quartz substrates with a roughness in the order of 50–100 micrometres were placed inside a quartz tube in the reactor at a temperature of approximately 900 °C. An Ar flow rate of 11 ml min^{-1} was used. The additional experiments were also performed in the presence of 2.5 mg sulfur and similar quantities of ferrocene. The radial structures were grown on the viscous boundary layer created between the rough surface of the quartz substrate and the Ar flow. The morphological characterization was performed through SEM and backscattered electrons (BE) with a JSM-7500F at 5–20 kV. The XRD analyses were performed with an Empyrean Panalytical diffractometer (Cu K-α with $\lambda = 0.154$ nm). The cross-sectional TEM, HRTEM, ED and STEM analyses were performed with a 200 kV American FEI Tecnai G^2F20. The magnetic properties were investigated through VSM at room temperature. The Raman scattering spectra were recorded in a Raman system using a triple grating monochromator (Andor Shamrock SR-303i-B, EU) with an attached EMCCD (ANDOR Newton DU970P-UVB, EU), with excitation by a solid-state laser at 532 nm (RGB lasersystem, NovaPro 300 mW, Germany) and collection by a 100×, 0.90 NA objective (Olympus, Japan). The FT-IR measurements were performed with a Nicolet 6700 in air.

Results and discussion

The morphology of the as grown radial structures was firstly revealed by SEM micrographs, as shown in Fig. 1. A typical top view of the as deposited radial structures after the cooling-stage is shown in Fig. 1A. It was noted that the radial structures were obtained in the form of thick deposits as the dominant product

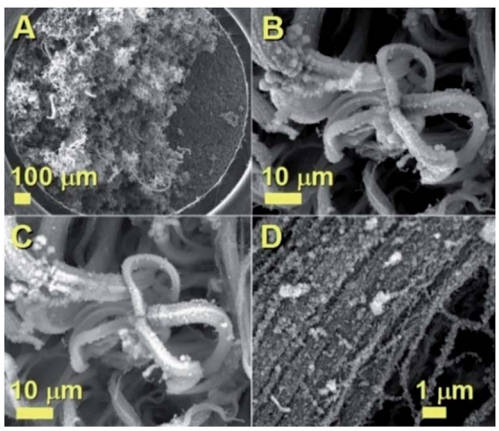

Fig. 1 SEM micrographs showing the morphology of the radial structures obtained by the pyrolysis of ferrocene/sulfur mixtures in the viscous boundary layer between the rough substrate surface and the Ar flow used.

in the reaction zone. These results also suggest that, in the presence of sulfur species, the viscous boundary layer can induce the homogeneous nucleation of particles and subsequent growth of radial CNT structures filled with continuous nanowires. A typical example of a radial CNT structure grown in the presence of sulfur is shown in Fig. 1B. Interestingly, these structures appear to be characterized by branches comprising numerous aligned CNTs. The evaluation of the filling rate was then considered using backscattered electrons. In Fig. 1C, the bright areas represent the region of high atomic number contrast (high metal content). The finer detail of a typical radial-structure branch can be observed in Fig. 1D. It seems clear that each branch consists of aligned CNT structures.

In order to further evaluate the filling rate of these structures, TEM, HRTEM and STEM were utilised. In Fig. 2A an example of the cross-sectional morphology of a radial structure is shown. In comparison with the radial structures produced with only ferrocene, a central core comprising an agglomeration of Fe_3C encapsulated nanoparticles was found. However in contrast to the previous reports, these particles are characterized by a much lower number of graphitic layers. The central core of the radial structure in Fig. 2A is shown with greater detail in Fig. 2B. The attention was then focused on the morphology of the CNT structures grown from the central-core. These analyses revealed that the majority of the CNTs within the radial structure are characterized by extremely high metal-filling rates. The encapsulated nanowires are found to be continuous and homogeneous for many micrometres along the CNTs capillary. Typical examples of the continuous nanowires can be observed in Fig. 2A and 4A in TEM mode, in Fig. 3, 5 and 6 in HRTEM mode and in Fig. 2C and 4B in STEM mode.

In particular the two red arrows in Fig. 2C show typical examples of many micrometres long nanowires encapsulated inside the CNTs. Fig. 2C and D also show with greater detail the STEM atomic contrast of the central cores of the radial

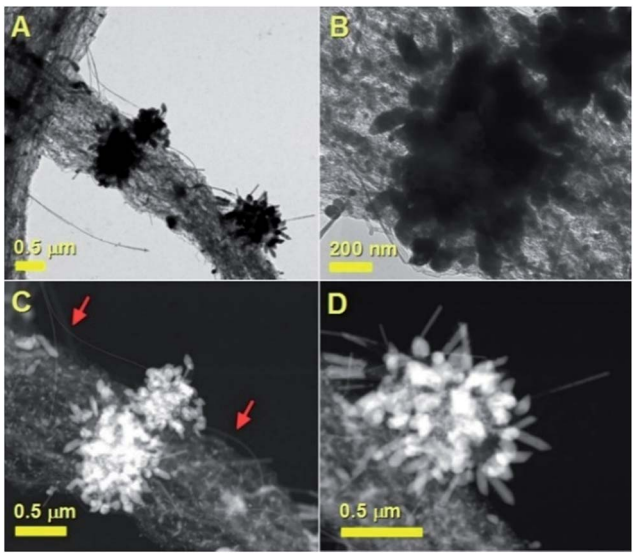

Fig. 2 Transmission electron micrographs (A and B) and scanning TEM (C and D) of typical radial Fe_3C filled thin walled CNTs.

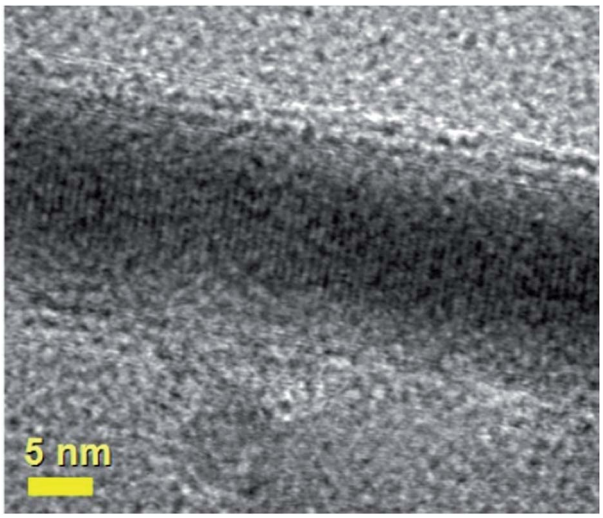

Fig. 3 HRTEM micrograph showing the preferred 010 reflection (lattice spacing of 0.67 nm) of a typical continuous Fe_3C nanowire encapsulated inside a thin walled CNT exhibiting 2–5 graphene-walls. See ESI† for energy dispersive X-ray analyses.

structures. Fig. 2D shows an example of a radial structure with multiple elongated nanowires departing from the central core. As shown in Fig. 3, in HRTEM mode, the CNT structures present a low number of walls (2–5 walls) and are filled with Fe_3C nanowires (observed 010 reflection of Fe_3C with space group *Pnma*). The single crystal arrangement of the nanowire is confirmed by the observation of a preferred 010 reflection of orthorhombic Fe_3C with space group *Pnma*.

It is important to notice that the Fe_3C nanowires embedded in our CNT sample present an unusual orientation with the 010 Fe_3C axis parallel to the CNT walls. Further confirmation of the continuous filling rate of the CNTs was given by other TEM analyses, as shown in Fig. 4A with TEM mode and in Fig. 4B with STEM mode. The use of selective area electron diffraction was also considered in order to better evaluate the presence of Fe_3C in the nanowire shown in Fig. 4A and B. These analyses (Fig. 4C) confirmed the presence of Fe_3C in single crystalline form (see caption of Fig. 4 for detailed indexing of the diffraction pattern reflections). In order to further investigate the orientation of the Fe_3C crystal shown in Fig. 4 along the CNT-capillary, further HRTEM analyses were considered. The HRTEM analyses of 3 different areas of the nanowire are shown in Fig. 5A and B and in Fig. 6. Interestingly (as described in detail in the caption of Fig. 5) a preferred orientation of the Fe_3C nanowire along the 010 crystal axis was found. This is confirmed also by the Fourier transform analyses of the HRTEM image in the inset of Fig. 5A. However, we notice also that a change in the orientation of the nanowire is present along the CNT capillary, as shown by the Fourier transform analyses of Fig. 5B and 6, where a change in the orientation of the 121 and 211 reflections (with respect to the CNT walls) is found.

The composition of the analysed Fe_3C nanowires was then evaluated through the use of energy dispersive X-ray spectroscopy. As shown in the ESI,†these analyses revealed the presence

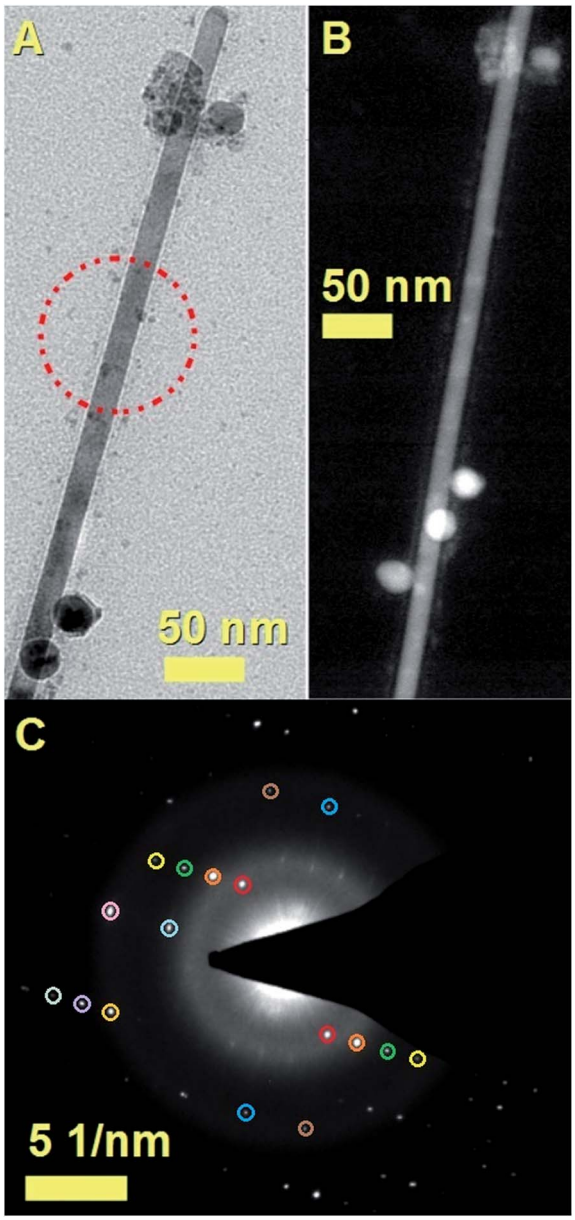

Fig. 4 Transmission electron and STEM micrographs in (A) and (B) showing a typical CNT completely filled with a Fe_3C nanowire. The single crystal arrangement is confirmed by the selective area electron diffraction pattern shown in (C). The reflection indexing was verified using kinematic scattering selection rules and dynamic scattering effects in the case of glide planes and/or screw axes. The observed reflections and extracted lattice spacings were as follows: 210 reflection (red circles, $d = 0.23$ nm); 221 reflection (orange circles, $d = 0.18$ nm); 222 reflection (green circles, $d = 0.146$ nm); 223 reflection (yellow circles, $d = 0.121$ nm); 040 reflection (cyan circle, $d = 0.16$ nm); 060 reflection (rose circle, $d = 0.11$ nm); 400 reflection (blue circles, $d = 0.13$ nm); 411 reflection (brown circles, $d = 0.12$ nm); 412 reflection (dark yellow circle, $d = 0.10$ nm); 422 reflection (purple circle, $d = 0.09$ nm); 440 reflection (light green circle, $d = 0.08$ nm).

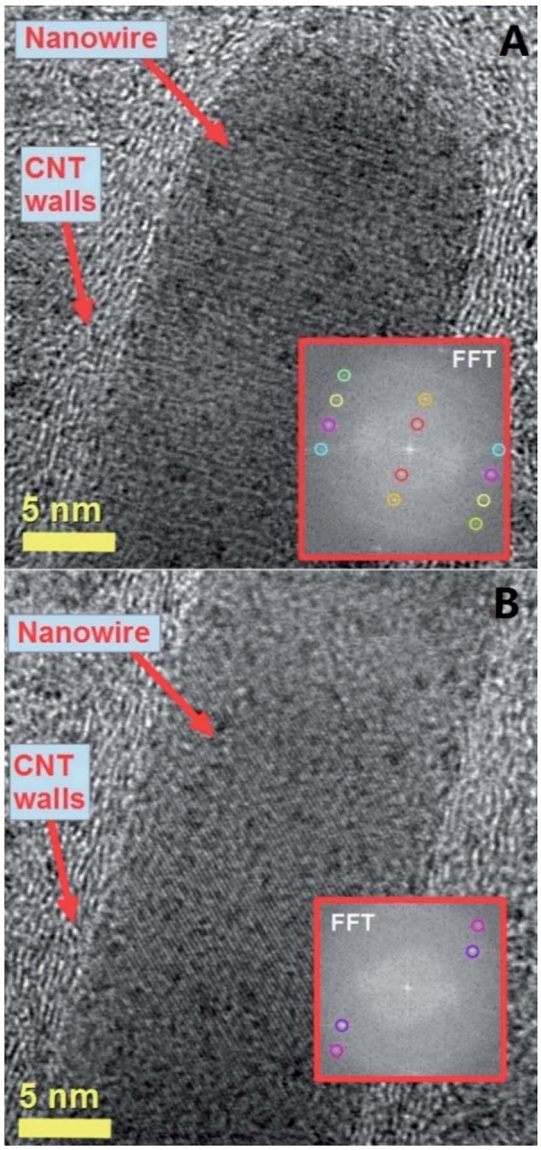

Fig. 5 High resolution transmission electron micrographs of a typical fully filled CNT in (A) and (B) showing the Fe_3C lattice spacings and fast Fourier transform of the lattice. The fast Fourier transform in the inset shows the reciprocal lattice spots corresponding to the reflections of Fe_3C with space group *Pnma*. In (A) the extracted Fe_3C reflections and lattice spacings from the inset are as follows: 010 reflection (red circles, $d = 0.68$ nm); 020 reflection (dark yellow circles, $d = 0.34$ nm); 102 reflection (magenta circles, $d = 0.21$ nm); 130 reflection (cyan circles, $d = 0.20$ nm); 031 reflection (yellow circles, $d = 0.20$ nm); 022 reflection (light-green circles, $d = 0.19$ nm). In (B) the extracted Fe_3C reflections and lattice spacings from the inset are as follows: 121 reflection (dark magenta circles, $d = 0.24$ nm); 211 reflection (pink circles, $d = 0.20$ nm).

of extremely low quantities of sulfur of 0.6%. These analyses are in agreement with those reported by Wei *et al.* in the case of empty CNTs grown in the presence of heterogeneously nucleated particles with tuneable quantities of sulfur.[32] The presence of Fe_3C as approximately single phase (90%) within the CNTs in the radial structures was also confirmed by additional XRD and Rietveld refinement analyses, as shown in Fig. S1.† These analyses also revealed the presence of very small quantities of γ-Fe and FeS_2. The observation of a low number of CNT walls can be attributed to the presence of sulfur species in the pyrolysed ferrocene vapour. Further examples of the radial-filled CNT

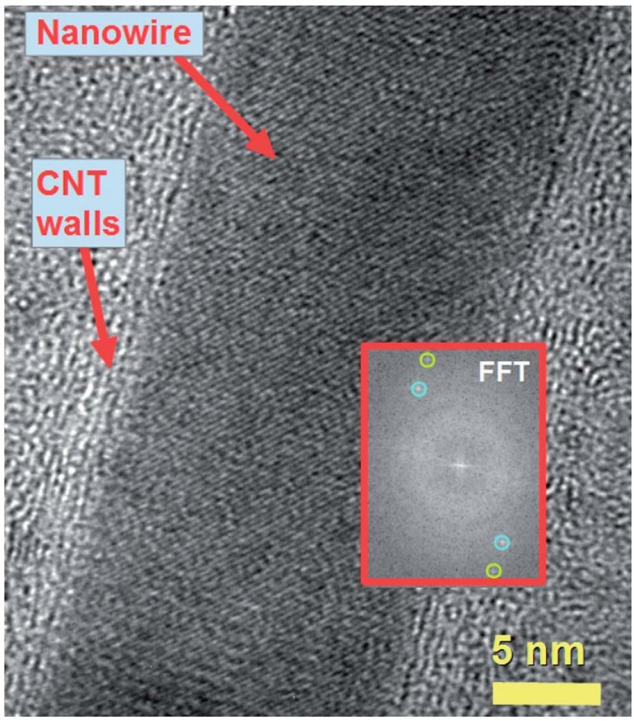

Fig. 6 High resolution transmission electron micrograph showing the lattice spacing and fast Fourier transform of the nanowire lattice. The fast Fourier transform in the inset shows the reciprocal lattice spots corresponding to the reflections of Fe_3C with space group *Pnma* as follows: 121 reflection (cyan circles, $d = 0.24$ nm); 211 reflection (green circles, $d = 0.20$ nm). Such lattice spacings have a different orientation with respect to those shown in Fig. 5A. This observation suggests that the Fe_3C nanowire does not always have the same orientation with respect to the CNT core.

structures can be found in Fig. 7. These analyses performed in STEM mode clearly prove further the high continuity of the nanowires (bright areas) encapsulated inside the CNTs (see Fig. 7A). Another typical example of the nanowire encapsulation inside the two thin-walled carbon nanotube structures is shown in Fig. 7B. The continuity of the bright areas proves the high quality of the encapsulated nanowires. Further confirmation of the CNT-wall crystallinity was then sought by Raman spectroscopy analyses.

As shown in Fig. S3 and S4†, the observation of the D and G bands in the regions of approximately 1300 cm^{-1} and 1600 cm^{-1}, together with the RBM modes in the region of 200 cm^{-1}, confirmed the presence of graphitic thin walls in the CNTs within the radial structures. Further confirmation of these analyses was then considered through the use of FT-IR spectroscopy. As shown in Fig. 8 these measurements revealed the presence of a peak in the region of approximately 1600 cm^{-1} which could be assigned to the contribution of the CNTs in the radial structures (note that previous studies also assigned this band to CNTs contribution).[33–35] The evaluation of the magnetic properties of the continuous nanowires in the radial structures was then considered though VSM analysis at room temperature. The results of the VSM analyses are shown in Fig. 9.

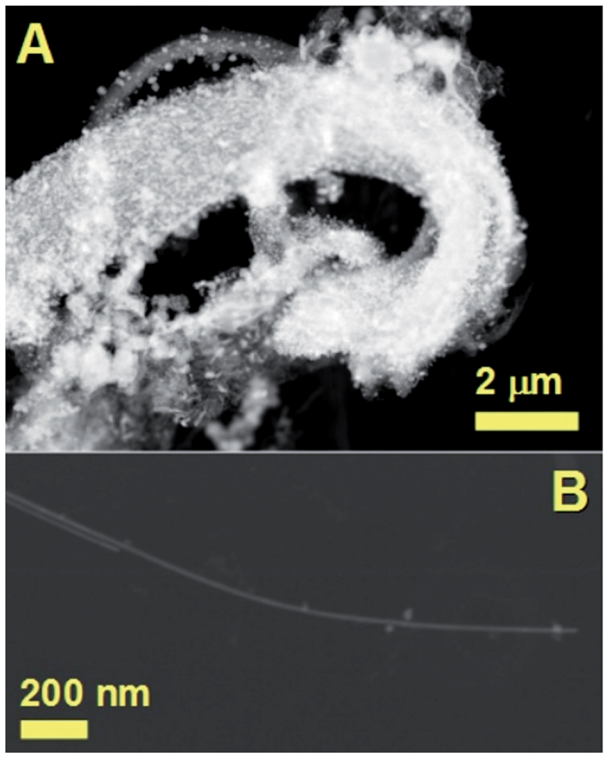

Fig. 7 STEM analyses showing more examples of the filled CNTs obtained by boundary layer CVS of ferrocene/sulfur mixtures.

These analyses revealed a saturation magnetization in the order of 35 emu g^{-1} and a coercivity of 400 Oe. The magnetic properties are comparable to those reported by R. Lv *et al.* in the case of thin walled CNTs filled with FeCoNi (approximately 35 emu g^{-1}) and FeNi (approximately 60 emu g^{-1}) nanowires.[18] These magnetic properties are also comparable to those reported by Boi *et al.* in the case of radial structures continuously

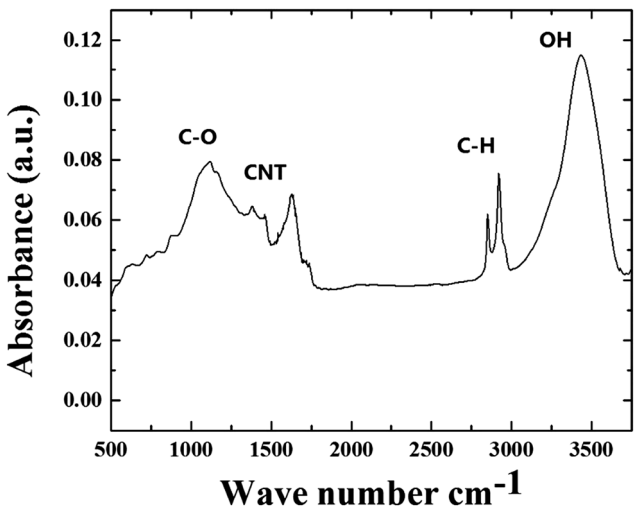

Fig. 8 FT-IR analyses (in air) of the radial filled thin walled CNT structures obtained by boundary layer CVS of ferrocene/sulfur mixtures.

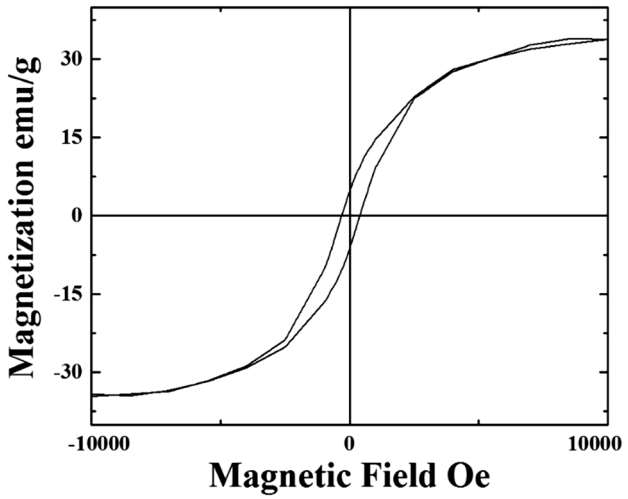

Fig. 9 VSM analyses at 300 K of the as grown radial few-wall CNT structures filled with continuous Fe_3C single crystals.

filled with Fe-based nanowires[10] and by Boi *et al.* in the case of thin walled CNT buckypapers (10–70 walls) highly filled with Fe_3C single crystals.[20] However note that in this work a much lower nanowire-diameter is observed. Also the coercivity of these structures is found to be comparable to that reported in the previous studies on thin walled CNTs filled with Fe_3C.

An evaluation of the radial structures' growth mechanism was then considered (see Fig. 10). This mechanism can be divided into several steps involving (1) the homogeneous nucleation of supersaturated Fe_3C particles in the viscous boundary layer as a consequence of critical Fe and C concentration in the perturbed viscous vapour and (2) the formation of agglomerates of spherical particles as a consequence of the perturbed flow-fluctuations in the boundary layer. Due to the presence of sulfur in the pyrolysed ferrocene vapour, the formation of eutectic Fe–S–Fe in the localised areas of the homogeneously nucleated particles is expected (the yellow areas in Fig. 10 show possible examples of the formation of this eutectic Fe-S-Fe). The presence of Fe–S–Fe eutectic phases induces a process of graphitization very different with respect to that described in the viscous boundary layer experiments performed with only ferrocene.[10] Indeed in this case, the formation of carbon islands (graphitization process) in both the homogeneously nucleated particles and Fe–S–Fe active areas can be considered. The nucleation of CNTs is expected to be promoted in the Fe–S–Fe eutectic areas. Indeed, the surface free energy of FeS at the eutectic temperature (1261 K) has been reported to be -84.17 kJ mol^{-1}. This value is much lower than that of α-Fe (-0.19 kJ mol^{-1}).[32] This difference implies that the activation energy for CNT nucleation from the Fe–S–Fe eutectic areas is much lower than that required from α-Fe. Thus, the nucleation of CNTs is most likely to occur on the lower free energy surface of eutectic Fe–S–Fe rather than on the pure Fe where a higher free energy surface is present.[32] As a consequence, the nucleated nanotube structures would have a diameter which is much smaller than that of the homogeneously nucleated particles in

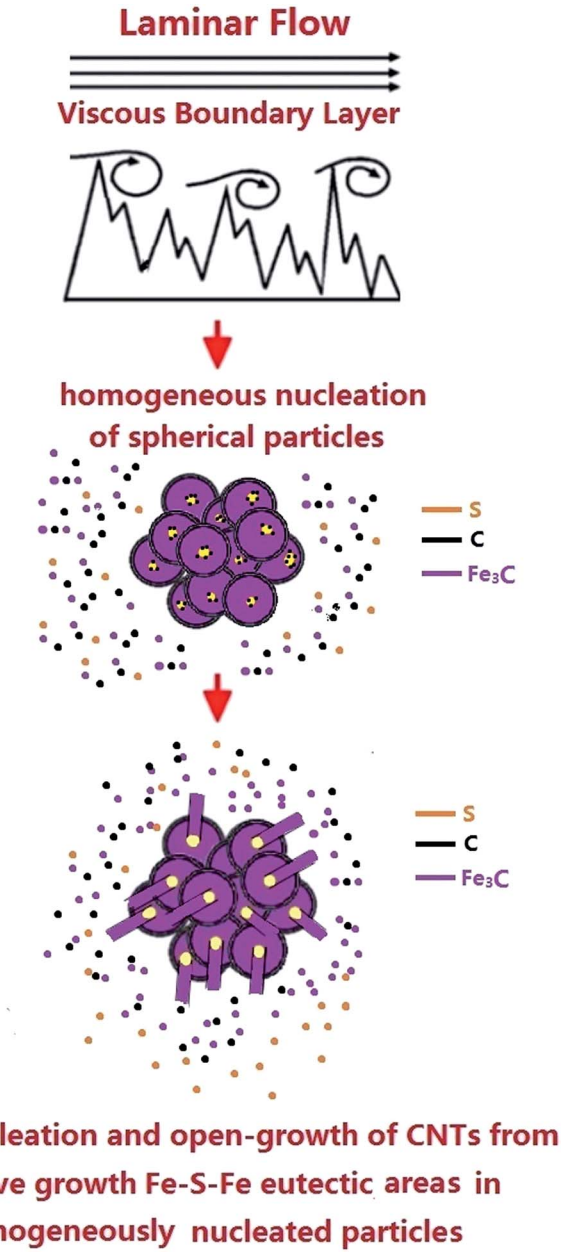

Fig. 10 Schematic showing the growth mechanism of the radial structures in the presence of sulfur species. The Fe–S–Fe eutectic active areas are shown in yellow.

the agglomeration. This difference can be attributed to the concentration of sulfur in the system and therefore to the size of the formed Fe–S–Fe active areas. This interpretation is confirmed also by statistical investigations of the CNT diameter, CNT-wall number and nanowire diameter, as shown in ESI Fig. S5–S12.† Indeed a dependence of the CNT-diameter and walls number on the sulfur concentration is found. This interpretation is partially in agreement with the growth mechanism proposed by Wei *et al.*[32] In addition, the observation of extremely high ferromagnetic filling rates strongly suggests that in our system, due to the presence of sulfur species, the growth of the radial structures is still driven by the presence of an open

growth mechanism at the tip of the CNTs in the radial structures (see schematic in Fig. 10).

In order to further confirm the dynamics of the proposed growth mechanism, additional experiments were also performed in the presence of a lower quantity (2.5 mg) of sulfur. The cross-sectional morphology of the radial structures obtained in these conditions is shown in Fig. 11A and B. Curiously, we find that the radial structures grown in these conditions are decorated with a large number of particles. As shown in the statistical investigations of Fig. S11 and S12,† when 2.5 mg of sulfur is used in the CVS reaction, the CNTs within the radial structures are found with a smaller diameter (in the order of 16 nm) and with a lower number of CNT walls (1–5 CNT walls). Typical examples of fully filled CNTs obtained in these conditions are shown in Fig. 12A and B in high resolution. Interestingly (see Fig. 12A and B and inset) also in these conditions, the Fe_3C nanowires are found with a variable orientation with respect to the CNT walls.

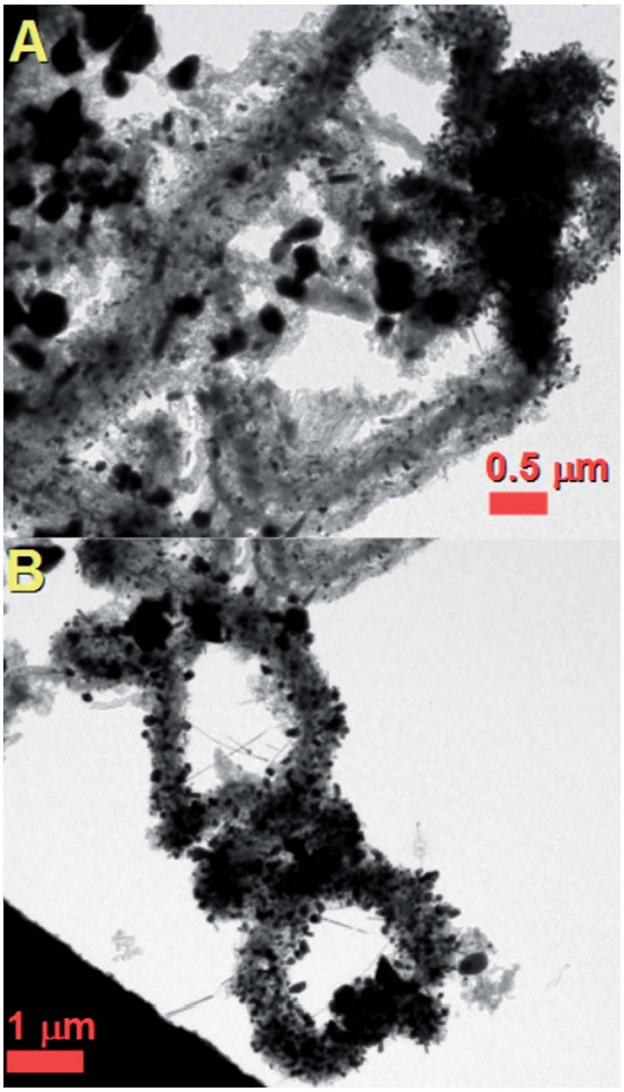

Fig. 11 Transmission electron micrographs (A and B) of typical radial Fe_3C filled thin walled CNT structures obtained by pyrolysis of ferrocene with 2.5 mg of sulfur.

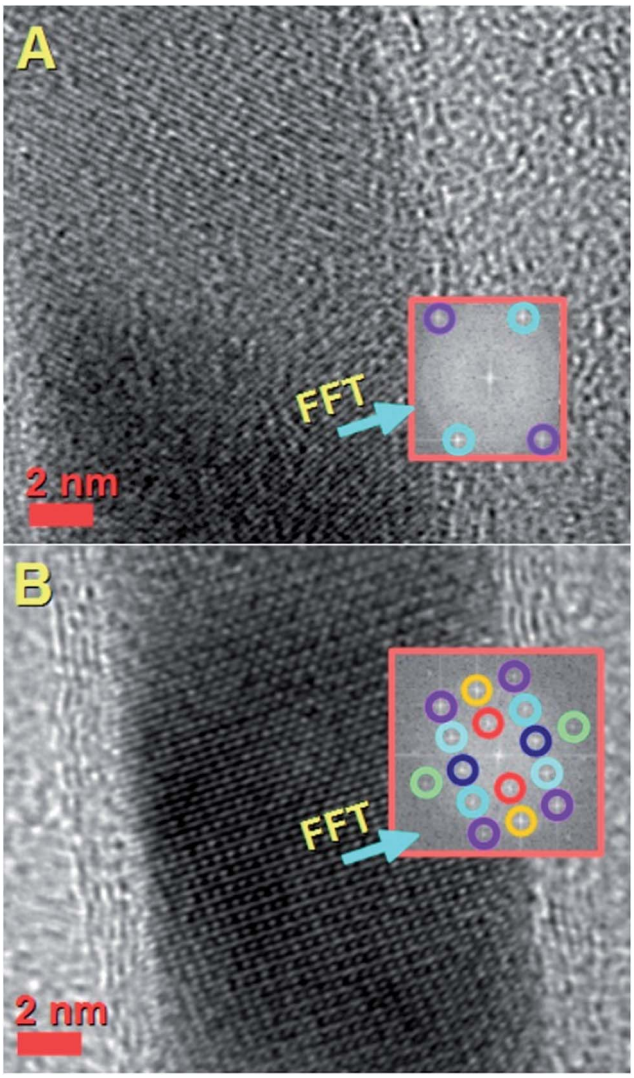

Fig. 12 High resolution transmission electron micrographs of a typical fully filled CNT in (A) and (B) showing the Fe_3C lattice spacing and fast Fourier transform of the lattice. The fast Fourier transform in the insets shows the reciprocal lattice spots corresponding to the reflections of Fe_3C with space group *Pnma*. In (A), the extracted Fe_3C reflections and lattice spacings from the inset are as follows: 121 reflection (cyan circles, $d = 0.24$ nm); 130 reflection (purple circles, $d = 0.21$ nm). In (B) the extracted Fe_3C reflections and lattice spacings from the inset are as follows: 100 reflection (red circles, $d = 0.50$ nm); 200 reflection (yellow circles, $d = 0.255$ nm); 001 reflection (dark blue circles, $d = 0.44$ nm); 002 reflection (green circles, $d = 0.22$ nm); 111 reflection (cyan circles, $d = 0.33$ nm); 201 and −201 reflections (purple circles, $d = 0.22$ nm).

Further examples of the fully-filled CNTs in the radial structures are shown in Fig. 13A and B. These analyses confirm the high quality of the filled CNTs produced with this growth method. However, we also notice that in the presence of 2.5 mg of sulfur, CNTs with a diameter in the order of 8 nm are present (see statistical analyses in ESI†). For such small CNT diameters an almost empty CNT-core is found. These observations may suggest that the open-growth mechanism, which favours continuous filling (as described above), is favourable for CNT diameters in the order of 11 nm or larger.

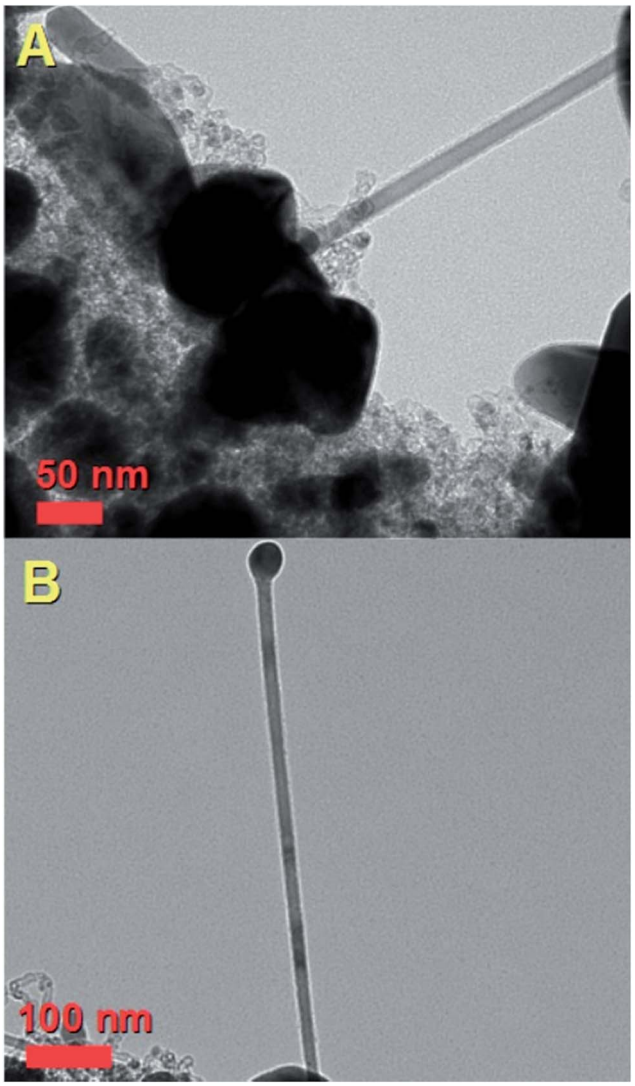

Fig. 13 Transmission electron micrographs (A and B) of typical fully-filled thin walled CNTs in the radial structures obtained by CVS experiments involving the pyrolysis of ferrocene with 2.5 mg of sulfur.

Conclusion

In conclusion, we reported the synthesis of novel radial few-wall carbon nanotube structures continuously filled with nm-thin continuous Fe_3C nanowires as the dominant reaction product by pyrolysis of ferrocene/sulfur mixtures in the viscous boundary layer between a rough surface and a laminar Ar flow at low flow rates of 11 ml min^{-1}. In many cases, the Fe_3C nanowires are found with an unusual orientation along the 010 axis. We have demonstrated that the addition of small quantities of sulfur in the viscous boundary layer has a dramatic effect on the growth mechanism of the radial structures, and this leads to a considerable decrease in the nucleated CNT-diameter and wall number. This is confirmed by the statistical analyses shown in the ESI (Fig. S5–S15†). We have analysed the morphology and crystallinity of the radial nanotube structures together with the continuity of the Fe_3C nanowires and single crystalline arrangement through the use of numerous techniques: SEM, TEM, HRTEM, ED, STEM, backscattered electrons, XRD, and Raman and FT-IR spectroscopy. The magnetic properties have been investigated through VSM. These results show promise for the possible future applications of radial filled few-wall carbon nanotube structures in thermoelectric systems, magnetic sensors, microwave absorption and other applications. Future work will focus on the development of these applications.

Acknowledgements

We acknowledge Prof. Gong Min for his continuous support, and the National Natural Science Foundation of China Grant No. 11404227.

Notes and references

1 S. Iijima, *Nature*, 1991, **354**, 56.
2 S. Iijima and T. Ichihashi, *Nature*, 1993, **363**, 603.
3 M. S. Dresselhaus, G. Dresselhaus and P. Avouris, *Carbon Nanotubes: Synthesis, Structure, Properties and Applications*, Springer, Berlin, 2001.
4 Z.-P. Yang, L. Ci, J. A. Bur, S.-Y. Lin and P. M. Ajayan, *Nano Lett.*, 2008, **8**, 446–451.
5 M. B. Bryning, D. E. Milkie, M. F. Islam, L. A. Hough, J. M. Kikkawa and A. G. Yodh, *Adv. Mater.*, 2007, **19**, 661–664.
6 J. Zou, J. Liu, A. S. Karakoti, A. Kumar, D. Joung, Q. Li, S. I. Khondaker, S. Seal and L. Zhai, *ACS Nano*, 2010, **4**, 7293–7302.
7 M. T. Byrne and Y. K. Gunko, *Adv. Mater.*, 2010, **22**, 1672–1688.
8 D. Wang, P. Song, C. Liu, W. Wu and S. Fan, *Nanotechnology*, 2008, **19**, 075609.
9 A. Leonhardt, M. Ritschel, D. Elefant, N. Mattern, K. Biedermann, S. Hampel, C. Muller, T. Gemming and B. Buchner, *J. Appl. Physiol.*, 2005, **98**, 074315.
10 F. S. Boi, G. Mountjoy and M. Baxendale, *Carbon*, 2013, **64**, 516.
11 F. S. Boi, G. Mountjoy, R. M. Wilson, Z. Luklinska, L. J. Sawiak and M. Baxendale, *Carbon*, 2013, **64**, 351–358.
12 T. Peci and M. Baxendale, *Carbon*, 2015, **98**, 519–525.
13 W. Wang, K. Wang, R. Lv, W. J. Zhang, X. Kang, F. Chang, *et al.*, *Carbon*, 2007, **45**, 1105–1136.
14 R. Lv, F. Kang, W. Wang, J. G. J. Wei, K. Wang and D. Wu, *Carbon*, 2007, **45**, 1433–1438.
15 R. Lv, A. Cao, F. Kang, W. Wang, J. Wei and J. Gu, *J. Phys. Chem. C*, 2007, **111**, 11475.
16 R. Lv, S. Tsuge, X. Gui, K. Takai, F. Kang, T. Enoki, *et al.*, *Carbon*, 2009, **47**, 1141–1145.
17 X. Gui, K. Wang, W. Wang, J. Wei, X. Zhang, R. Lv, *et al.*, *Mater. Chem. Phys.*, 2009, **113**, 634–637.
18 R. Lv, F. Kang, J. Gu, X. Gui, J. Wei, K. Wang, *et al.*, *Appl. Phys. Lett.*, 2008, **93**, 223105.
19 J. Guo, M. Lan, S. Wang, Y. He, S. Zhang, G. Xiang, *et al.*, *Phys. Chem. Chem. Phys.*, 2015, **17**, 18159–18166.

20 F. S. Boi, J. Guo, S. Wang, Y. He, G. Xiang, X. Zhang and M. Baxendale, *Chem. Commun.*, 2016, **52**, 4195–4198.
21 J. M. Romo-Herrera, B. G. Sumpter, D. A. Cullen, H. Terrones, E. Cruz-Silva, D. J. Smith, V. Meunier and M. Terrones, *Angew. Chem., Int. Ed.*, 2008, **47**, 2948.
22 J. M. Romo-Herrera, D. A. Cullen, E. Cruz-Silva, D. Ramirez, B. G. Sumpter, V. Meunier, H. Terrones, D. J. Smith and M. Terrones, *Adv. Funct. Mater.*, 2009, **19**, 1193.
23 H. W. Zhu, C. L. Xu, D. H. Wu, B. Q. Wei, R. Vajtai and P. M. Ajayan, *Science*, 2002, **296**, 884.
24 J. Q. Wei, B. Jiang, D. H. Wu and B. Q. Wei, *J. Phys. Chem. B*, 2004, **108**, 8844.
25 T. Luo, L. Y. Chen, K. Y. Bao, W. C. Yu and Y. T. Qian, *Carbon*, 2006, **44**, 2844.
26 J. Ma, J. N. Wang and X. X. Wang, *J. Mater. Chem.*, 2009, **19**, 3033.
27 X. X. Wang, J. N. Wang and L. F. Su, *J. Power Sources*, 2009, **186**, 194.
28 J. Q. Huang, Q. Zhang, F. Wei, W. Z. Qian, D. Z. Wang and L. Hu, *Carbon*, 2008, **46**, 291.
29 L. Song, L. Ci, L. Lv, Z. Zhou, X. Yan, D. Liu, H. Yuan, Y. Gao, J. Wang, L. Liu, X. Zhao, Z. Zhang, X. Dou, W. Zhou, G. Wang, C. Wang and S. Xie, *Adv. Mater.*, 2004, **16**, 1529–1534.
30 W. Ma, L. Song, R. Yang, T. Zhang, Y. Zhao, L. Sun, Y. Ren, D. Liu, L. Liu, J. Shen, Z. Zhang, Y. Xiang, W. Zhou and S. Xie, *Nano Lett.*, 2007, **7**, 2307–2311.
31 W. Zhou, Q. Fan, Q. Zhang, K. Li, L. Cai, X. Gu, F. Yang, N. Zhang, Z. Xiao, H. Chen, S. Xiao, Y. Wang, H. Liu, W. Zhou and S. Xie, *Small*, 2016, **12**, 3407–3414.
32 J. Wei, H. Zhu, Y. Jia, Q. Shu, C. Li, K. Wang, B. Wei, Y. Zhu, Z. Wang, J. Luo, W. Liu and D. Wu, *Carbon*, 2007, **48**, 2152–2158.
33 A. Misra, P. K. Tyagi, P. Rai and D. S. Misra, *J. Nanosci. Nanotechnol.*, 2007, **7**, 1820–1823.
34 N. Kouklin, M. Tzolov, D. Straus, A. Yin and J. M. Xu, *Appl. Phys. Lett.*, 2004, **85**, 4463–4465.
35 D. B. Mawhinney and J. T. Yates Jr, *Carbon*, 2001, **39**, 1167–1173.

